Composites Science and Technology 216 (2021) 109060

Contents lists available at ScienceDirect

Composites Science and Technology

journal homepage: www.elsevier.com/locate/compscitech

"Un-forming" fibre-steered preforms: Towards fast and reliable production of complex composites parts

Xiaochuan Sun *, Jonathan P.-H. Belnoue, Wei-Ting Wang, Byung Chul Kim, Stephen R. Hallett

Bristol Composites Institute (ACCIS), University of Bristol, Queen's Building, University Walk, Bristol, BS8 1TR, UK

ARTICLE INFO

Keywords:
A. Structural composites
A. Polymer-matrix composites (PMCs)
C. Finite element analysis (FEA)
C. Deformation
Automated fibre placement

ABSTRACT

Automated Fibre Placement (AFP) allows for efficient deposition of composite prepreg materials at large scale in a reliable and reproducible way, while keeping human effort to a minimum. However, the technique is not perfectly suited to manufacturing small/medium parts with complex geometries. Deviation between as-designed and as-manufactured parts is almost inevitable, as is the occurrence of process-induced defects. In this study, an alternative design and manufacturing process is proposed. Instead of depositing composite tapes directly onto the complex mould, a flat tailored preform made from steered fibre tows is created first, and then the flat preform is subsequently formed into a 3D complex shape. The fibre path in the flat tailored preform is derived from a new virtual 'un-forming' process of a complex 3D part design with target fibre paths. To demonstrate the process, a small doubly curved composite part was un-formed. Fibre-steered tailored preforms were created using the continuous tow shearing (CTS) technique and then formed into the target shape using double diaphragm forming. The as-manufactured part was compared with the as-designed part as well as a part manufactured from straight fibre prepreg. The results demonstrated the feasibility of the virtual un-forming process and the potential of proposed manufacturing route.

1. Introduction

In the past two decades, the increasing demand for carbon fibre reinforced composites in the aerospace industry has been a key driver of the development and improvement of automated composite deposition [1]. Automated fibre placement (AFP) is the most widespread automated composite manufacturing technique, efficiently integrating multiple processes into a single step. One of the major benefits from AFP is the key role it has played in the advancement of variable angle tow (VAT) composites where fibre reinforcements are steered along optimised curvilinear trajectories. VAT laminates allow for broadening the design space and improvements in composites' load-bearing capability through tailoring of stress distribution for structural applications [2–5]. State-of-the-art AFP machines accept both dry fibre and prepreg tapes with width ranging from 1/8″–1″. The combination of the steering capability and the ability to deposit narrow tapes enables AFP systems to manufacture large and simply contoured structures (e.g. fuselage in Boeing 787 and Airbus A350 wing skins [6]) and has helped considerably in widening the range of application of composite structures.

However, many of the advantages of AFP become less obvious and lead to manufacturing defects when laying-up over a highly doubly curved surface and around tight radius. In these cases, the outer and inner edges of the tape are subjected to different stress states and the compressive stress generated along the inner edge of the tape results in out-of-plane wrinkles leading to poor layup quality which ultimately impacts the structural performance of the parts [7–10]. AFP processes involve fibre tapes being (pre-) heated, deposited and consolidated by a roller along a pre-defined path. Consequently, many machine parameters need to be adjusted (i.e. roller material, compaction pressure, temperature of the heating element, deposition speed etc.) and can all affect the final quality of the layup. Understanding how each of these parameters and their combination impact the layup quality is an

* Corresponding author.
E-mail address: ric.sun@bristol.ac.uk (X. Sun).

https://doi.org/10.1016/j.compscitech.2021.109060
Received 13 May 2021; Received in revised form 12 September 2021; Accepted 20 September 2021
Available online 23 September 2021

extremely complex task and the easiest way to decrease the appearance of defects is often to simply slow down the deposition speed [9], particularly when directly laying-up on complex (i.e. doubly curved) 3D surfaces. In the cases where manufacturing defects are observed, the layup is often completely reworked. The time required for inspection and rework can normally take up to 63% of the overall process window, even exceeding the laydown time, and ultimately leads to high running costs and material wastage [11].

An alternative manufacturing technique to AFP is the forming of fibrous sheets (prepreg or dry) onto a 3D mould [12]. The part thickness can be built up by forming either each layer one by one (i.e. sequentially) or forming a prebuilt multi-layer stack directly [13,14]. The main advantage of forming over the AFP process directly onto the mould is its high material deposition rate. However, if the fibre paths in the preforms are straight, forming would lead to significant deviation between the fibre paths in the physical manufactured part and the design intent, where the optimal fibre orientations often form curved paths on the mould surface. This deviation results in less efficient structural designs and consequently an unnecessarily large safety factor. In addition, in a similar way to what is seen during the steering process in AFP, forming often leads to the generation of defects such as in-plane and out-of-plane wrinkles, which further impact the structural performance of the parts. As the preform is formed onto the mould, it is deformed to accommodate the change of shape. The near inextensibility of the fibres generates internal constraints in the preform material that may prevent the required distortions and thus lead to fibre path deviation away from the design intent. Other factors such as stacking sequence for multi-ply laminates and ambient forming temperature also profoundly influence the forming process and defect generation, and their significance was analysed in [14,15].

In this study, the feasibility of a novel manufacturing technique, where automated ply deposition and forming are combined, was demonstrated. A unique automatic ply deposition process that quickly lays up onto a flat tool whilst steering fibres was used to create custom preforms that can then be formed to the required shape in 3D. The fibre paths in the flat preform were determined using a novel un-forming, i.e. a reversed forming, simulation. The proposed technology is defined by three key steps (see Fig. 1):

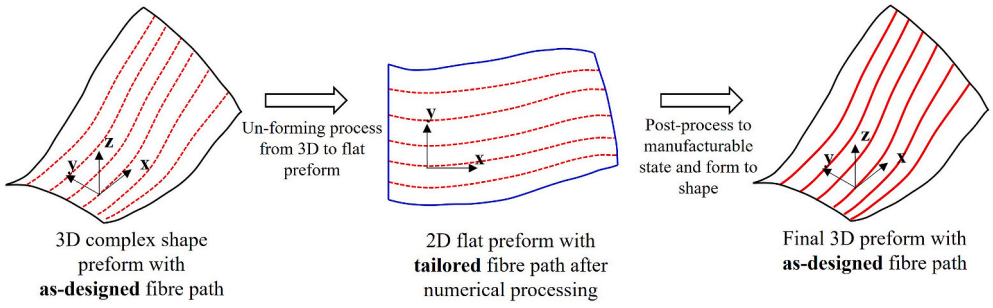

Fig. 1. Schematic of un- and forming processes in 'lay-flat and form'.

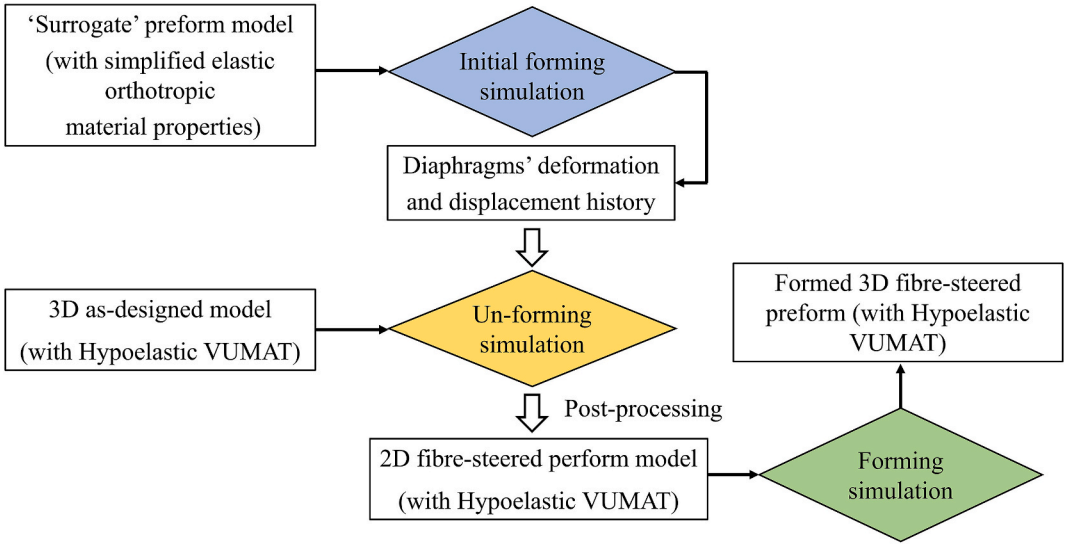

Fig. 2. General workflow chart of modelling used in this study. Note that line arrows indicate direct output or input within corresponding model and hollow arrows indicate post-processing between different steps.

- ***Generating the 2D tailored preform design from the target 3D fibre path:***

This is achieved through a novel numerical simulation approach that derives the required fibre orientation in the flat tailored preform via the "un-forming" of the as-designed part with target 3D fibre paths.

- ***Continuous Tow Shearing (CTS) process to create fibre-steered preforms:***

This process is an evolution from AFP that has been proven to minimise steering defects. The method allows for the creation of a steered preform by continuously shearing the fibre tows or tapes instead of bending them as in conventional AFP. The detailed description of the CTS process can be found in [16].

- ***Forming the fibre-steered preforms into the finished 3D part:***

The tailored preforms with steered fibre paths obtained in previous step is then formed on a mould of the required 3D shape using double diaphragm forming technique [17].

The numerical process by which the fibre orientation in the flat tailored preform is obtained holds some similarities with previous work from Rudd et al. [18], in which an optimised flat preform was derived via an concept of un-draping process (modified kinematic draping) from a 3D hemisphere geometry. Kinematic draping is a widely used tool to approximate fibre orientation during fabric draping onto complex 3D surfaces and is normally based on the pin-jointed net concept, with assumptions of inextensible fibre tow, zero preform shear stiffness and absence of process constraints [19]. In this work, a finite element analysis (FEA) based method, which accounts for the real physics of the problem (including prepreg material behaviour and boundary conditions), was used instead of a kinematic drape algorithm. This allows the fibre paths in the flat preform to be directly derived from only one un-forming simulation (i.e. no optimisation cycles are required in the case of the geometry studied here). Hence the final fibre orientations after forming, derived from a forming simulation, should show only small deviation from the targeted design. In addition to the improvements in laminate quality and production rate, the method also reduces waste compared to parts manufactured through forming of straight fibre plies.

This work is an expanded investigation based on previous study [20] in which the proof of concept and general workflow were initially demonstrated. The manuscript is organised in a chronological order from process modelling development to experimental demonstration. Section 2 provides a description of the simulation platform used to calculate the orientation of the fibre paths in the flat preform and the un-forming analysis. Section 3 reports the experimental work carried out to demonstrate the feasibility of the numerical technique. Finally, Section 4 discusses and concludes on the viability of the technique by comparing the results from the analysis, with the experimental measurements and the original design requirements.

2. Numerical modelling

2.1. General modelling strategy

In order to better present the entire process and each simulation's input and output, a workflow chart of the model strategy is illustrated in Fig. 2, in which line arrows indicate direct input or output within the corresponding model and hollow arrows indicate post-processing between different steps that were outlined in previous section.

An important factor in the forming of fibrous material is the boundary conditions applied to the preform. Even the two identical preforms being formed on the same tool through a forming process with a blank-holder and a double diaphragm forming (DDF) respectively will display fundamentally different wrinkle patterns due to the different tension on the preform [21]. These are typical manufacturing induced defects that a simpler kinematic modelling approach [18,22] would not be able to capture. There is, therefore, a strong need for a more accurate FE-based approach that can capture these load-path dependencies.

In the present study, DDF was selected due to several of its merits. It is capable of multi-layer forming, which is ideal for low cost and high-volume applications; secondly manufacturing defects generated from it and processing pressure present some similarities to industrial process such as hot drape forming [23,24]. Another benefit of DDF is the reduction of material wastage as, unlike forming with a blank holder, no excess preform material is required to be constrained during forming, which makes net-shaped preforms a possibility. In addition, the effect of the boundary conditions given by the blank holder on the forming response of a preform is complex in nature, and computationally expensive to simulate [25,26].

Because of the complex effect of boundary conditions and their influence on the stress built up within the preform, setting-up an un-forming process model is not straightforward. Furthermore, the deformed shape of the diaphragm material after forming is unknown and cannot be used in a process where the boundary conditions of a forming process are simply inverted. A remedy was found by setting-up a procedure as described as follows (see Fig. 2): first an initial DDF process modelling of a 'surrogate' preform with representative material properties was carried out; then the reversed nodal displacement history of the diaphragm finite element model was then applied as a displacement field input to the simulation of the un-forming process, and finally the 'surrogate' preform is replaced by a material model with more realistic properties. Forming of the fibre-steered preform was finally performed

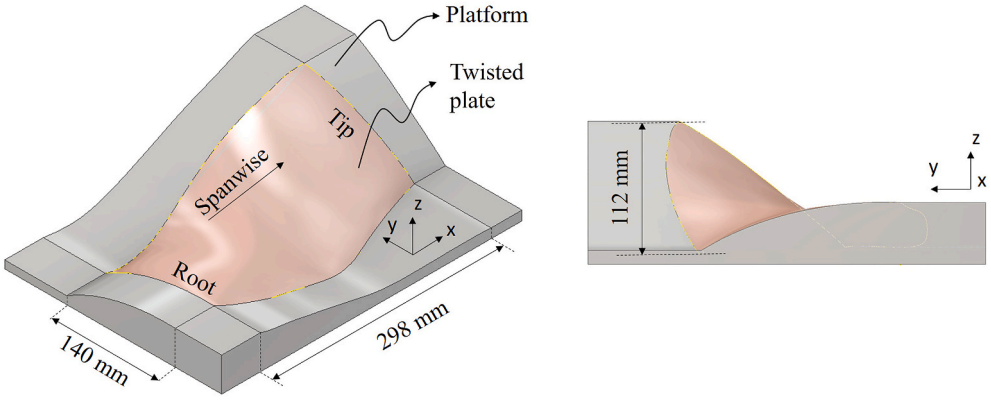

Fig. 3. Designed mould with basic dimensions and the twisted plate part is highlighted in the centre of the mould.

to check if the fibre orientation in the formed fibre-steered part was consistent with the as-designed part (the 3D as-designed preform model). The un-forming and forming simulations were carried out using the commercial FE package (Abaqus/Explicit) with user defined material model (VUMAT).

2.2. Mould and sample design

To demonstrate the advantages of the proposed process and to validate the model, a twisted, swept and doubly curved 3D surface (referred as "twisted plate" hereafter) was designed and manufactured. Fig. 3 shows basic dimensions and overall configuration of the mould. The region that extends from the twisted plate's edges serves as a 'platform' to prevent the preform from being folded around the edges and corners of the mould during forming. The CAD geometry was built and then imported into Abaqus for further processing. Only the top surface of the virtual 3D mould was modelled and meshed with rigid material properties and membrane elements, respectively, to reduce computational cost. The CAD geometry of the top surface of designed mould was then again used Abaqus separately, to model the as-designed preform part.

2.3. Finite element modelling

2.3.1. Model set-up

The chord, in some areas of the twisted plate, varies along the span direction. This is problematic as simple structured mesh scheme (i.e., when the numbers of elements along chord direction are the same) does not allow the spanwise elements to have a constant width (chordwise), which could be made equal to the width of a steered fibre tow. To define the as-designed spanwise fibre path, the preform mesh was thus created with an in-house Python script that kept the true 3D width of each spanwise strip of elements constant and equal to the width of a fibre tow. These strips of elements represent the as-designed fibre tow paths on the part, and their elemental orientation represents the fibre orientation on the as-designed 3D part. Note that the way of deriving the as-designed 3D part design used in this study was inspired by a general design rule of maximising the amount of continuous fibre running in spanwise from root to tip in order to retain good structural performance of part under centrifugal force. In the context of this manuscript, it only served as a 'target' fibre orientation that the un-forming modelling started from. To accurately capture the material behaviour of the preform during the forming/un-forming process, an approach that was initially developed for the modelling of forming of woven fabric [21] and then later developed for capturing in-plane shear response of UD prepreg [27] was adopted here.

Reduced-integration shell elements (S4R in Abaqus/Explicit) and membrane elements (M3D4R in Abaqus/Explicit), with size of 4 mm, were superimposed by sharing their nodes, to represent the out-of-plane bending and in-plane material properties of the preform, respectively. The Young's moduli in the shell and membrane elements were set to different values in such a way that membrane elements were used to simulate the in-plane behaviour (extension in fibre and transverse directions and in-plane shear) of a unit area of the preform whilst the shell elements were used to represent the fabric out-of-plane bending behaviour. The Young's modulus of shell elements was back calculated from the flexural rigidity of the preform and the transverse and in-plane properties were set to small values. The membrane and shell elements thicknesses were both set to the actual preform thickness (i.e. 0.25 mm).

Table 1
Material input parameters for the elements in the thermoset prepreg model.

Element type	E_1 (MPa)	E_2 (MPa)	G_{12} (MPa)	Thickness (mm)
Membrane	149	10	5	0.25
Shell	33	5	0	

Specific values of the Young's moduli of the membrane and shell elements are given in Table 1. These elements collectively simulate the complete material behaviour of a prepreg sheet. This approach works well for both woven fabrics and unidirectional prepregs [21,27].

To accurately represent the orthotropic nature of the material during forming where rigid body rotation can be significant, the constitutive behaviour of the preform was implemented based on a hypoelastic material model via a VUMAT material subroutine in Abaqus/Explicit. A local 2D orthogonal coordinate system in the Green-Naghdi (GN) work frame (i.e. Abaqus VUMAT work frame that elemental strain input and stress output are calculated from) is defined, and fibre direction relative to this local coordinate is set as VUMAT inputs. During forming simulations, this coordinate system is subject to a rigid body rotation which is represented by a rotation tensor $\mathbf{R}$, this rotation tensor can be decomposed by polar decomposition i.e. $\mathbf{R} = \mathbf{F}\cdot\mathbf{U}^{-1}$, where $\mathbf{F}$ is the deformation gradient and $\mathbf{U}$ is the right stretch tensor for internal straining of the material. A rotated local coordinate system can then be derived via the rotation tensor $\mathbf{R}$ from its initial state. With knowing the current deformation gradient, the deformed fibre direction can be calculated. Strain increments received by the VUMAT under the GN work frame are then converted to the fibre direction work frame for constitutive calculation while stress increments as output from the VUMAT in the fibre direction work frame are then converted back to the GN work frame for next iteration. Further Details of this material model are not elaborated in here as they can be found in the supplementary information and [21]. This VUMAT subroutine is made freely available by Bristol Compos Institute (BCI) and can be requested by e-mailing bci-github@bristol.ac.uk.

Ogden's hyperelastic material model with representative parameters given in [17,21] and S4R elements, with element size of 4 mm, were assigned and used for modelling the diaphragms. The material parameters used are listed in Table 2.

2.3.2. Un-forming and forming simulations

As mentioned in Section 2.1, the un-forming process model was implemented by directly reversing the forming process. As un-forming cannot be physically realised with a separate experimental validation, the whole process (i.e. un-forming and forming simulations) was validated by comparing the predicted fibre orientation of the formed preform with that of the physical demonstrator in the as-designed state. Good agreement between these different cases proved the validity of the proposed method. As shown in Fig. 2, an initial forming simulation was first carried out. Displacement histories of the diaphragms' nodes were extracted and stored. When simulating the un-forming process, the nodal displacement histories obtained from the initial forming simulation were assigned to the diaphragms' nodes in the opposite direction and reversed time history. This allows both diaphragms to be deformed back to their original flat states.

As shown in Fig. 4a, the initial forming simulation model consists of four parts, i.e. two diaphragms, the mould and a 'surrogate' preform. During the initial forming, contact interaction (including friction) between the diaphragms and the preform may affect the deformation pattern as different materials respond differently when they are formed into the same shape. To take the tangential interactions between diaphragms and preform into account, Coulomb friction coefficients of 0.6 and 0.52 was assigned at interfaces between diaphragms and diaphragm-preform, respectively. These values were experimental determined in [17] and used in similar simulation works in [17,28].

Table 2
Material parameters for Ogden hyperelastic material model used for the diaphragm material, from [17,21]. Parameters μ_1, α_1 and μ_2, α_2 are material constants derived by curve fitting of uniaxial and biaxial tension tests.

Diaphragm material	μ_1 (Pa)	α_1	μ_2(Pa)	α_2
Thermoplastic elastomer	150,904	3.0918	813.392	0.81451

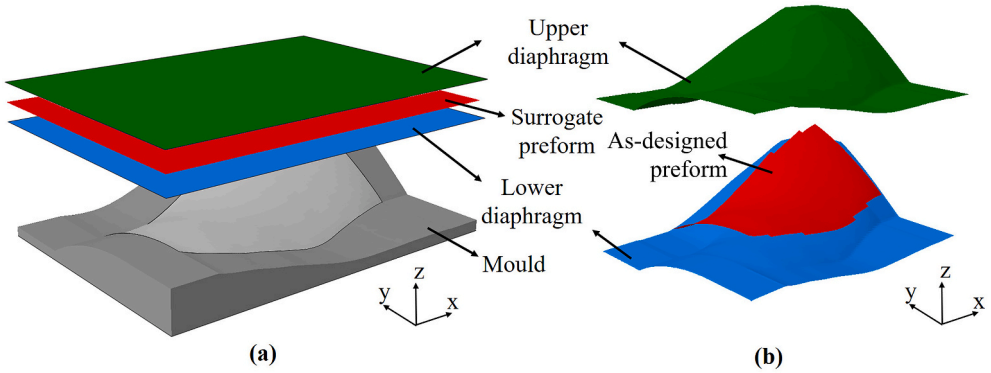

Fig. 4. Illustration of (a) initial forming model, (b) un-forming model. Note that the diaphragms' position relative to the mould and the preform and the size of the preform are for presentation only.

The 'surrogate' preform model used in the initial forming simulation allows to obtain more accurate diaphragm movement by considering diaphragm/diaphragm and diaphragm/preform interactions, as well as the effects of the bending behaviour of the preform on diaphragms' deformation. A simplified elastic orthotropic material model with unidirectional fibre orientation aligned with the plate span was used. The assumption here is that the effects of steered fibre (i.e. preform bending) is small with respect to the diaphragm interactions. Small differences observed in the deformation of diaphragms in forming simulations of preforms with straight and steered fibres respectively presented later show that this assumption is reasonable. The diaphragms' deformation and their interaction with the preform can be significantly complex for multiply preform forming onto a complex mould in which it is anticipated that the benefits from using this surrogate preform will become even greater. It may be that in such a case, an iterative forming-unforming process will be needed in order to reach the required preform design.

At the end of this initial forming simulation, the diaphragms and 'surrogate' preform fully conformed to the top of the mould. Their deformed shapes were then used as the initial configuration of the un-forming simulations (see Fig. 4b). In particular, an anisotropic material with the fibres' orientation set as in the as-designed preform model was placed between diaphragms in the un-forming model. Hence, the as-designed 3D preform is deformed by the double diaphragms during un-forming from the twisted shape with element orientations along the as-designed fibre tow paths (as-designed preform in Fig. 4b) to a flat tailored preform with steered fibre paths.

Material properties used in the initial and un-forming simulations as well as the model validation experiment are listed in Table 1. However, the in-plane shear behaviour and transverse deformation of prepreg is strongly influenced by deformation rate (forming rate in this case). During forming process of 3D complex moulds, different deformation rates will occur at different locations on the preform, which will be affected by the viscoelastic nature of the material [27,29]. The resin-dominated mechanical properties are also highly sensitive to temperature and can vary significantly [29]. Therefore, it is worth noting that the material properties listed in Table 1 and those used in simulations were representative and limited to the case studied in here,

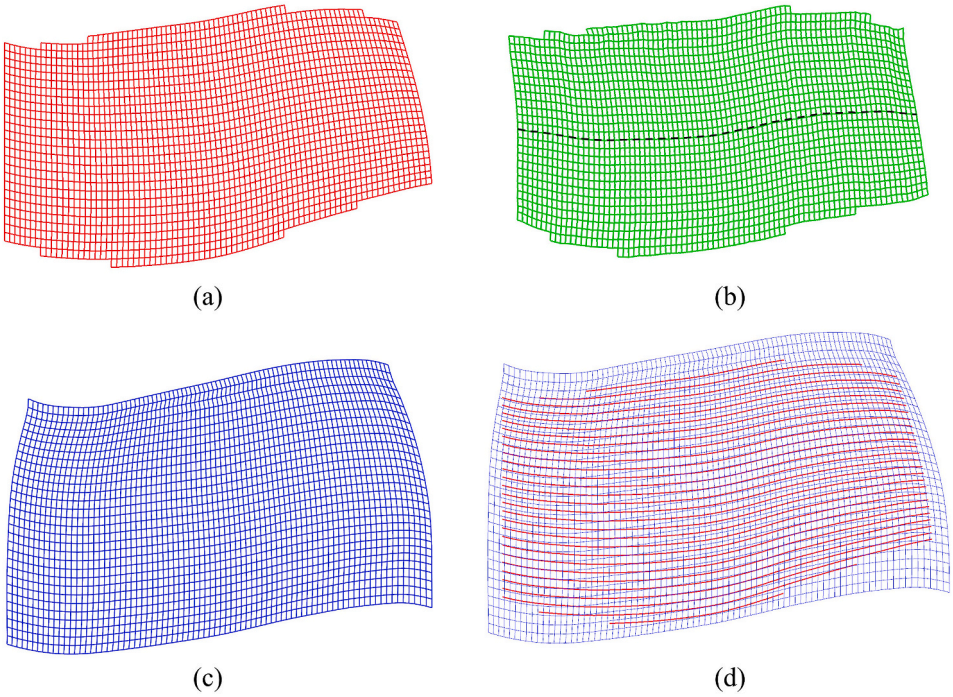

Fig. 5. Top views of: (a) trimmed as-designed preform model, (b) 2D fibre-steered preform model with extracted fibre path at mid-chord in 2D, (c) formed 3D fibre-steered preform model, (d) comparison of fibre path between the 3D as-designed preform and the formed 3D fibre-steered preform model. Note that each model in this figure correspond to the simulation workflow chart in Fig. 2.

and they would require update based on material characterisation testing and given testing facilities or manufacturing environment for forming of other complex shapes with different materials.

As mentioned in Section 2.3.1, shear modulus (G_{12}) or variation of shear modulus against shear angle in membrane element can be specified in the hypoelastic VUMAT material model to capture in-plane shear behaviour of preform during forming simulation [21,29]. In this work, the shear modulus of the membrane elements was given an notional value that is much lower than that tested for a similar material in [29], and this low shear modulus was expected to introduce more in-plane shear in the preform to test the robustness of the post-processing tools. However, for the given shape in this work, the numerical and experimental results showed that the material deformations, including transverse extension and in-plane shear, were insignificant to the overall result. In general, because of the orthotropic nature of prepreg, the fibre and transverse direction bending response of the prepreg, captured by shell elements in the hypoelastic VUMAT material model, were significantly different. Therefore, the flexural stiffnesses of the UD prepreg used in the study were also representative and require cantilever bend characterisation tests such as presented in [21,30] to obtain precise properties for future analyses.

As a result of deriving the as-designed 3D part with elemental orientation aligned with the required fibre orientations from the initial structural mesh, each strip of chordwise elements do not terminate exactly at the edges of the original boundary of the twisted plate region. Elements beyond the boundary were trimmed, thus the overall size of the part was preserved. Fig. 5a shows the as-designed preform model in 3D and its mesh, processed from the initial structural mesh. After the un-forming simulation, to avoid any localised response (i.e. residual in-plane shear) in the un-formed tailored preform model (see Fig. 5b) and to make it manufacturable for fibre steering in experiment, the un-formed preform was further processed and re-meshed by a custom developed Python script so that spanwise strips of elements have a constant width, representing a CTS-manufacturable preform. It is worth noting that the numerical procedure described here would work in the exact same way for fibre-steering in AFP. Finally, the fibre-steered preform was then formed and compared with the original 3D as-designed preform as shown in Fig. 5c and d, respectively. It is worth noting that the un-formed 2D fibre-steered preform model (see Fig. 5b), based on the as-designed preform model, was trimmed to fit to the surface of the mould but could not precisely cover the entire surface of the mould due to its mesh size and shape, therefore, it was slightly smaller than the mould surface. The 3D fibre-steered preform model used in the forming simulations (see Figs. 5c and 2) was meshed based on a single fibre trajectory extracted from the un-formed preform and its base span and chord were set to be equal to the maximum span and chord of the mould surface. This leads to the size of the formed fibre-steered preform to be slightly larger than the mould surface and, by extension, the formed fibre-steered preform to be larger than the 3D as-designed preform, as shown in Fig. 5d.

All numerical models were processed by with 16 CPUs, and the initial forming and tailored preform forming models were completed in under 30 min with appropriate mass scaling and damping to reduce dynamic effects. In the un-forming simulation, nodal displacement histories derived from initial forming simulation were written out in the form of text files and taken as boundary conditions in the un-forming model. The time required for these text files to be read into memory (~30 min) was longer than the actual simulation time of the un-forming model (~15 min). An efficient file exchange procedure may help to speed up the overall computational time even further.

3. Experiments

In this work, an experimental demonstrator of the proposed manufacturing technique was produced, and the results were used to validate the process models presented in Section 2.

A single fibre path was extracted from the mid-chord position of the simulated tailored preform design, as shown in Fig. 5b. A steered prepreg preform was then manufactured by the CTS technique using the extracted fibre path (see Fig. 6). The exceptionally small minimum steering radius of the CTS process allowed for production of such small fibre-steered preforms without defects. Since the width of the designed part is about 140 mm, two 100 mm wide prepreg tapes (MTM49-3/T800, Solvay, BE) along the preform width were deposited onto a flat surface in the CTS process. To capture the fibre path with an image processing and make quantitative comparison between the preforms before and after forming, white lines parallel to the fibre directions were marked at 20 mm intervals on the prepreg tapes before it was fed into the CTS machine. The fibre path in a 2D cartesian coordinate format from the FEA results was converted to a CTS machine code, using a previously developed method from Kim et al. [31,32]. In addition, a double diaphragm forming test was carried out using a single UD prepreg sheet with 0° fibre orientation aligned with the long edge of the plate was carried out. This allowed for highlighting the benefits of the proposed method compared with a more conventional manufacturing technique using straight fibre preforms.

A double diaphragm forming rig was designed and built to accommodate a small-to medium-sized tooling mould. Fig. 7a illustrates a cross-sectional view of the forming rig. During forming, the preform was placed between two diaphragms and held by a clamping frame on top of the upper diaphragm along the edges of the forming chamber. Prior to forming, 1 bar vacuum pressure was applied between the diaphragms and held throughout the forming process. After the preform was correctly positioned and secured between the diaphragms, the forming chamber was evacuated under 1 bar pressure for forming (see Fig. 7a). The mould, with a geometry identical to the numerical model used in the simulation, was manufactured by 3D printing (Fused Deposition Modelling) and was found to provide sufficient support. It was placed at centre of the forming rig. The peripheral areas between forming chamber and mould were filled with solid high-density Styrofoam blocks which were trimmed into shapes to avoid sharp corners and ensure a smooth surface transition between the forming chamber and the mould.

Fig. 7b shows an overview of the forming rig with a formed fibre-steered prepreg. Due to twist of the mould, the relative position of the mould to the forming chamber was also one of the key influencing factors to forming quality, as it affects the change of the contact area

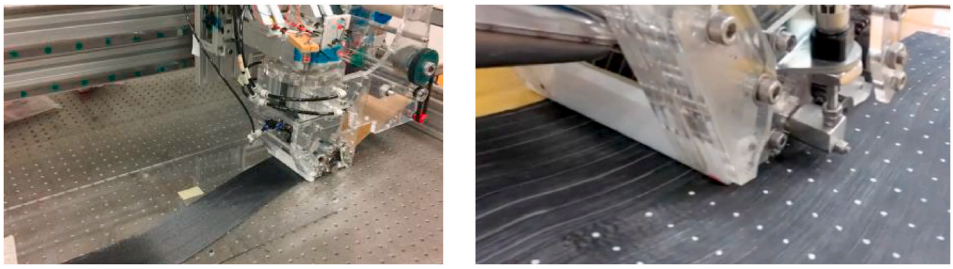

Fig. 6. Overview of CTS machine (*left*) and wide tape CTS machine steering a 100 mm wide unidirectional prepreg tape (*right*).

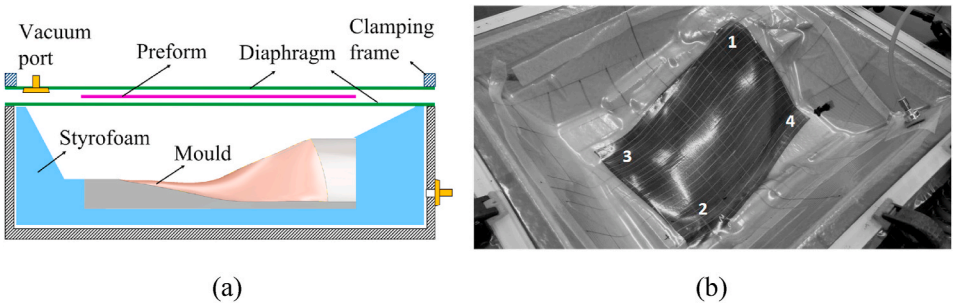

Fig. 7. (a) Cross-sectional schematic of the forming rig with exploded view showing the position of diaphragms and preform; (b) overview of forming rig with formed prepreg and forming sequence. (the numbers indicate the order in which forming of each part is completed.)

between the diaphragm and the mould during forming. For forming using a single preform in this study, due to the low modulus in the transverse direction (in-plane normal to fibre orientation) of the preform, tension applied by the diaphragm during forming can be detrimental to preserve the steered fibre directions. To minimise this tensioning effect on the preform, the mould was placed in such a way that the forming sequence is along the fibre direction from the apex to the bottom corners of the mould, as shown by the numbers in Fig. 7b.

A DSLR (digital single-lens reflex camera) camera was placed on a supporting frame above the forming rig focusing downward to the centre of the preform; images were taken after the preform was completely formed to the mould. These images were then post-processed for fibre path extraction.

4. Results and discussions

Numerical simulations of the initial forming, un-forming and forming of tailored preform were carried out according to the modelling strategy described in the Section 2. To reduce computational cost in the forming and un-forming simulations, the complete forming rig used in experiments was not modelled entirely, and the forming process was instead modelled by altering the pressure acting on the diaphragms. During forming simulations, the same uniform pressure distribution was applied to both diaphragm models in the opposite directions. Similarly to the modelling techniques found in [17,21], after the diaphragms and preform are stabilised, the pressure acting on the lower diaphragm was gradually reduced to 80% of its original value so that the double diaphragms and preform model were simultaneously formed onto the mould.

Fig. 5b shows the un-formed tailored preform derived from the un-forming simulation with the fibre trajectory highlighted. Because highly localised shear deformation was not observed, a single trajectory was sufficient to represent the fibre path for the entire preform, and this fibre trajectory was extracted and used to manufacture a fibre-steered preform using CTS. Fig. 5d compares the 3D formed tailored preform with the 3D as-designed preform. It can be seen that the predicted fibre

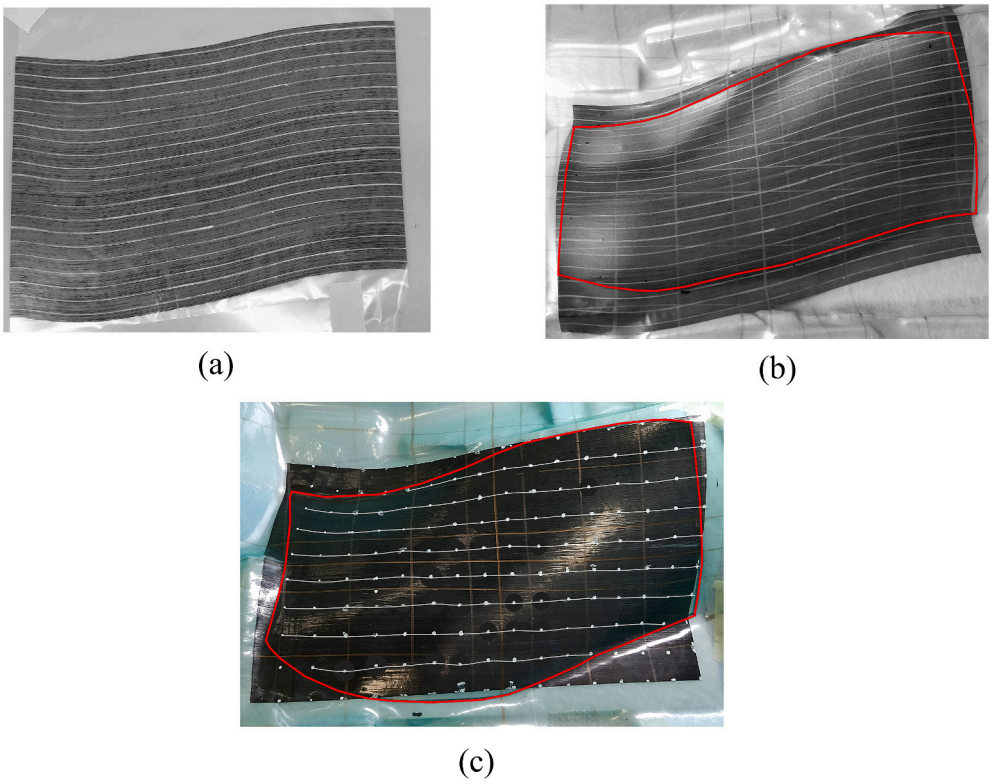

Fig. 8. (a) Flat preform deposited by CTS machine with fibre direction highlighted, (b) CTS preform (fibre-steered) formed onto twisted plate mould, (c) UD preform (straight fibre) formed onto twisted plate mould by double diaphragm forming, with white lines indicating fibre orientation and the boundary of the twisted plate mould highlighted in red. (For interpretation of the references to colour in this figure legend, the reader is referred to the Web version of this article.)

path (represented by strips of elements) in the formed tailored preform is in good agreement with the original as-designed preform.

Fig. 8a shows the flat preform deposited by the CTS machine. After the preform was manufactured, it was then transferred to the forming rig to form into shape. Fig. 8b shows the formed CTS preform. It can be seen from the figure and during the forming test, splitting between the two parallel 100 mm wide fibre tapes at the joined boundaries was not observed, which showed efficiency and robustness of the CTS technique in manufacturing defect-free preforms. Several trials were required before the preform could successfully be formed to the shape with full coverage and with a good alignment to the peripheral of the mould. Hence, each position in the tailored preform uniquely corresponds to one position on the mould. A visual assisting tool such as a projector above the forming rig could be helpful to align preform to the mould in future work. The occurrence of slippage between diaphragms and preform during forming can also affect the forming quality, and it is caused by relieving the compression acting on the preform leading to local relaxation of preform. This slippage was expected to be associated with prepreg tack, modulus mismatch of the two materials, vacuum pressure between the diaphragms and the boundary conditions of the diaphragms. To check for the occurrence of preform slippage against the diaphragms during forming, trials were carried out with the top diaphragm marked by grid lines. However, no diaphragm slippage was observed experimentally. Friction between diaphragms affects their relative movement in the tangential direction but does not significantly affect deformation in regions that are in contact with the preform. There are other factors that control the interaction between diaphragms, such as uniformity of vacuum pressure, type of diaphragm, boundary conditions, ambient temperature (some forming tests may require elevated temperature), etc. The level of characterisation performed here was deemed to be sufficient for the studied problem.

In other multiply forming cases where the moulds are even more complex than that in current study, a full numerical sensitivity study of the interfacial properties for diaphragms and diaphragm/preform and interply interactions may be required. The importance of these interactions varies from case to case and requires in-situ observation and bespoke numerical characterisation/validation based on the given preform stack, diaphragm type, mould shape, boundary conditions, forming facility, test environment, etc.

As mentioned in Section 3, the same forming test was performed with a UD prepreg sheet. Fig. 8c shows the formed UD prepreg with gridlines drawn before the forming test to indicate the fibre orientation before and after forming. The boundary of the twisted plate is also highlighted on the figure. Comparison between Fig. 8b and c shows that when using the UD preform, a large amount of material needed to be trimmed to fit to the required (highlighted) surface, which leads to production of waste. The UD preform also has a reduction of continuous spanwise fibre running from the root and the tip of the shape. However, in the formed CTS preform, the amount of continuous fibres was greater and trimming could be kept to a minimum. This demonstrates the advantages of the steered preform in forming of complex shapes. It is also noted that the tailored steered fibre preform appeared to be easier to form. This suggest that, in the case of more aggressive mould surface profiles, the technique may, as intended, help reduce the occurrence of defects. More importantly, this novel approach allows for manufacturing variable angle tow designs in such small and highly complex parts without defects, which is not possible using the conventional AFP process. This will enable high-volume production of more structurally efficient, complex composite components at reduced cost and waste.

For a more quantitative validation of the process models and of the proposed manufacturing approach, the deviation of fibre trajectories to the as-designed fibre paths in the FE forming simulations (see final step in Fig. 1) was compared with that in the physical demonstrator. As it was difficult to experimentally extract the fibre paths “in-situ” in 3D, the top view images of the as-designed preform obtained from the FE simulations were precisely overlaid to the corresponding images of the formed steered preform. Image processing scripts were developed to extract lines from an image and compare the deviation of fibre trajectories. The projected fibre orientations, i.e. marked lines on steered preform, were compared with the FEA mesh lines in the as-designed preform, as shown in Fig. 9a. A similar comparison was also made between the as-designed preform and the formed UD preform (see Fig. 9b). It can be seen that the fibre angle deviations observed over most of the area of the steered preform was below 5°, while higher values were found at the corner of the preform, which was caused by misalignment of the initial position of the steered preform before it was formed to the shape. For the purpose of proof of concept, the current validation process was deemed to be sufficient as a foundation for future studies.

5. Conclusions

In this work a manufacturing process, particularly well adapted to the production of complex 3D composites structures, is proposed. Instead of depositing carbon fibres directly on the complex mould, a flat tailored preform made from steered fibre prepreg tapes was created. The flat preform was, subsequently, formed into a 3D complex shape. The fibre path in the flat, tailored preform is derived from a new virtual un-forming process from the as-designed part. The fibre-steered preforms were created using the continuous tow shearing (CTS) technique and formed into shape using double diaphragm forming.

FEA process models and in-house scripts were developed for deriving as-designed fibre paths on arbitrary, yet complex shapes, the results of which were validated by forming of a fibre-steered preform. It was shown that a flat, custom fibre-steered preform could be obtained for the as-designed fibre paths via a numerical un-forming simulation. It was also observed that the part manufactured by the proposed process was

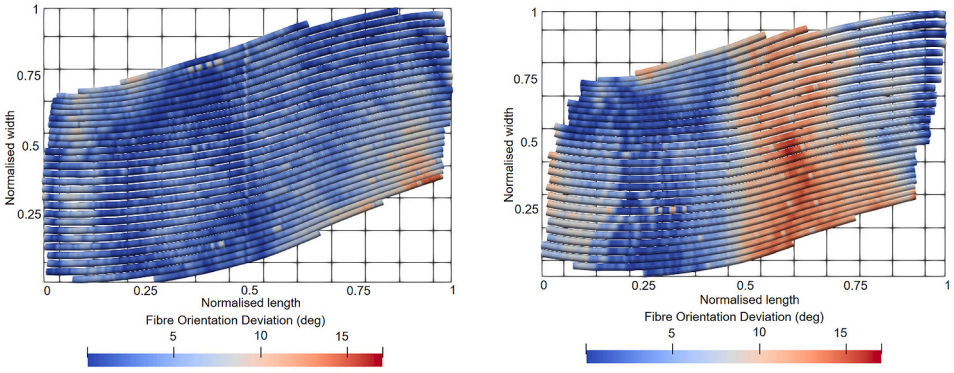

Fig. 9. Deviation of the experimental projected fibre trajectories between (a) the formed steered preform and the preform with as-designed fibre trajectory derived in FEA; (b) the UD preform and preform with as-designed fibre trajectory derived in FEA.

closer to the as-designed part and required less material compared to a part manufactured through forming of a UD preform. This proposed process effectively decouples a complex or even impossible process (i.e. direct AFP on small to medium complex surface) into two easily manageable processes. Hence, flat steered preform are first created using CTS and then formed to the required 3D shape. The 'un-forming' simulation allows to derive a tailored near net-shape preform. Compared with a more traditional AFP deposition, the technique can help lower trial-and-error iterations and reduce material waste.

Longer term, the technique could be fully automated by integrating the CTS machine into a process chain whereby steered fibre preforms are manufactured and moved to a forming station via pick and place. DDF is also a highly scalable process that uses vacuum only to generate forming forces and is both fast and cost-effective. Both one shot DDF multi-ply forming of the preforms or ply-by-ply sequential single diaphragm forming are viable options to build the part thickness onto the tool.

This proposed approach is believed to be suitable for manufacturing small to medium composite parts with complex shapes, which are not currently manufacturable using AFP processes directly. The un-forming simulation is applicable to all 3D shapes, but the numerical fibre-steered preforms generated may not always be manufacturable by current fibres steering processes. If fibre-steering technology becomes inadequate to produce such preforms, information from numerical fibre-steered preforms and from intermediate steps during the un-forming simulation can also be useful in creating optimised lay-up design for the purpose of reducing manufacturing defects.

Furthermore, the proposed method allows for applying novel variable angle tow designs to such complex shapes for more advanced performance, that could not previously be achieved for such small parts due to limitations of current AFP technologies. However, the application of this approach to even smaller and more complex mould than that used in this study may lead to small fibre steering radii during deposition, which requires further investigation in future studies based on the development of the CTS process. The new method's extension to deal with parts of increasing complexity of shape and multi-ply forming, including at elevated temperatures, will be studied in the future.

Credit authors contribution statement

Xiaochuan Sun: Methodology, Software, Investigation, Formal analysis, Validation, Writing – original draft, Visualization. Jonathan P.-H. Belnoue: Conceptualization, Writing – review & editing, Supervision. Wei-Ting Wang: Investigation. Byung Chul Kim: Writing – review & editing, Supervision. Stephen R. Hallett: Conceptualization, Writing – review & editing, Supervision, Funding acquisition

Declaration of competing interest

The authors declare that they have no known competing financial interests or personal relationships that could have appeared to influence the work reported in this paper.

Acknowledgements

This work was funded by the feasibility study "Virtual un-manufacturing of fibre-steered preforms for complex geometry composites" of the EPSRC (The Engineering and Physical Sciences Research Council, United Kingdom) Future Composites Manufacturing Hub (EP/P006701/1) and the EPSRC platform grant "SIMulation of new manufacturing PROcesses for Composite Structures (SIMPROCS)", (EP/P027350/1).

Appendix A. Supplementary data

Supplementary data to this article can be found online at https://doi.org/10.1016/j.compscitech.2021.109060.

References

[1] K.C. Wu, B.K. Stewart, R.A. Martin, ISAAC Advanced Composites Research Testbed. CAMX 2014 - Compos Adv Mater Expo Comb Strength Unsurpassed Innov, 2014.
[2] Z. Guerdal, R. Olmedo, Composite laminates with spatially varying fiber orientations - "Variable stiffness panel concept, in: 33rd Struct. Struct. Dyn. Mater. Conf., American Institute of Aeronautics and Astronautics, Reston, Virigina, 1992.
[3] Lukaszewicz DH-JAHJA, C. Ward, K.D. Potter, The engineering aspects of automated prepreg layup: history, present and future, Compos. B Eng. 43 (2012) 997–1009.
[4] Z. Wu, P.M. Weaver, G. Raju, B.C. Kim, Buckling analysis and optimisation of variable angle tow composite plates, Thin-Walled Struct. 60 (2012) 163–172.
[5] Z. Wu, G. Raju, P.M. Weaver, Postbuckling analysis of variable angle tow composite plates, Int. J. Solid Struct. 50 (2013) 1770–1780.
[6] A. Hiken, The evolution of the composite fuselage - a manufacturing perspective, SAE Int J Aerosp 10 (2017) 2017, 01–2154.
[7] W. Woigk, S.R. Hallett, M.I. Jones, M. Kuhtz, A. Hornig, M. Gude, Experimental investigation of the effect of defects in Automated Fibre Placement produced composite laminates, Compos. Struct. 201 (2018) 1004–1017.
[8] F. Heinecke, C. Willberg, Manufacturing-induced imperfections in composite parts manufactured via automated fiber placement, J Compos Sci 3 (2019) 56–80.
[9] J.P.-H. Belnoue, T. Mesogitis, O.J. Nixon-Pearson, J. Kratz, D.S. Ivanov, I. K. Partridge, et al., Understanding and predicting defect formation in automated fibre placement pre-preg laminates, Compos Part A Appl Sci Manuf 102 (2017) 196–206.
[10] O. Falcó, C.S. Lopes, J.A. Mayugo, N. Gascons, J. Renart, Effect of tow-drop gaps on the damage resistance and tolerance of Variable-Stiffness Panels, Compos. Struct. 116 (2014) 94–103.
[11] D. Maass, Progress in automated ply inspection of AFP layups, Reinforc Plast 59 (2015) 242–245.
[12] P. Boisse, J. Colmars, N. Hamila, N. Naouar, Q. Steer, Bending and wrinkling of composite fiber preforms and prepregs. A review and new developments in the draping simulations, Compos. B Eng. 141 (2018) 234–249.
[13] P. Wang, N. Hamila, P. Boisse, Thermoforming simulation of multilayer composites with continuous fibres and thermoplastic matrix, Compos. B Eng. 52 (2013) 127–136.
[14] D. Leutz, M. Vermilyea, S. Bel, R. Hinterhölzl, Forming simulation of thick AFP laminates and comparison with live CT imaging, Appl. Compos. Mater. 23 (2016) 583–600.
[15] K.J. Johnson, R. Butler, E.G. Loukaides, C. Scarth, A.T. Rhead, Stacking sequence selection for defect-free forming of uni-directional ply laminates, Compos. Sci. Technol. 171 (2019) 34–43.
[16] B.C. Kim, K. Potter, P.M. Weaver, Continuous tow shearing for manufacturing variable angle tow composites, Compos Part A Appl Sci Manuf 43 (2012) 1347–1356.
[17] S. Chen, O.P.L. McGregor, A. Endruweit, M.T. Elsmore, D.S.A. De Focatiis, L. T. Harper, et al., Double diaphragm forming simulation for complex composite structures, Compos Part A Appl Sci Manuf 95 (2017) 346–358.
[18] C.D. Rudd, M.R. Turner, A.C. Long, V. Middleton, Tow placement studies for liquid composite moulding, Compos Part A Appl Sci Manuf 30 (1999) 1105–1121.
[19] C. Krogh, B.L.V. Bak, E. Lindgaard, A.M. Olesen, S.M. Hermansen, P.H. Broberg, et al., A simple MATLAB draping code for fiber-reinforced composites with application to optimization of manufacturing process parameters, Struct. Multidiscip. Optim. 64 (2021) 457–471.
[20] X. Sun, J.P.-H. Belnoue, B.C. Kim, W.-T. Wang, S. Hallett, Virtual un-manufacturing of fibre-steered preforms for complex geometry composites, Procedia Manuf 47 (2020) 197–201.
[21] A.J. Thompson, J.P.-H. Belnoue, S.R. Hallett, Modelling defect formation in textiles during the double diaphragm forming process, Compos. B Eng. 202 (2020) 108357.
[22] S.G. Hancock, K.D. Potter, Inverse drape modelling—an investigation of the set of shapes that can be formed from continuous aligned woven fibre reinforcements, Compos Part A Appl Sci Manuf 36 (2005) 947–953.
[23] J. Sjölander, P. Hallander, M. Åkermo, Forming induced wrinkling of composite laminates: a numerical study on wrinkling mechanisms, Compos Part A Appl Sci Manuf 81 (2016) 41–51.
[24] P. Hallander, M. Akermo, C. Mattei, M. Petersson, T. Nyman, An experimental study of mechanisms behind wrinkle development during forming of composite laminates, Compos Part A Appl Sci Manuf 50 (2013) 54–64.
[25] A. Rashidi, H. Montazerian, A.S. Milani, Slip-bias extension test: a characterization tool for understanding and modeling the effect of clamping conditions in forming of woven fabrics, Compos. Struct. 260 (2021) 113529.

[26] J. Krebs, D. Bhattacharyya, K. Friedrich, Production and evaluation of secondary composite aircraft components - a comprehensive case study, Compos Part A Appl Sci Manuf 28 (1997) 481–489.
[27] Y. Wang, J.P.-H. Belnoue, D.S. Ivanov, S.R. Hallett, Hypo-viscoelastic modelling of in-plane shear in UD thermoset prepregs, Compos Part A Appl Sci Manuf (2021) 106400.
[28] A.J. Thompson, B. El Said, J.P.-H. Belnoue, S.R. Hallett, Modelling process induced deformations in 0/90 non-crimp fabrics at the meso-scale, Compos. Sci. Technol. 168 (2018) 104–110.
[29] Y. Wang, M.K. Chea, J.P.-H. Belnoue, J. Kratz, D.S. Ivanov, S.R. Hallett, Experimental characterisation of the in-plane shear behaviour of UD thermoset prepregs under processing conditions, Compos Part A Appl Sci Manuf 133 (2020) 105865.
[30] P. Harrison, Modelling the forming mechanics of engineering fabrics using a mutually constrained pantographic beam and membrane mesh, Compos Part A Appl Sci Manuf 81 (2016) 145–157.
[31] B.C. Kim, P.M. Weaver, K. Potter, Computer aided modelling of variable angle tow composites manufactured by continuous tow shearing, Compos. Struct. 129 (2015) 256–267.
[32] B.C. Kim, E. Zympeloudis, Improvement of fibre placement accuracy in continuous tow shearing process, 20th Int Conf Compos Mater 19–24 (2015).